Pulsed Plasmoid Propulsion: Air-Breathing Electromagnetic Propulsion
IEPC-2011-015

David Kirtley, John Slough, and Chris Pihl
MSNW LLC, Redmond, WA 98052, USA

Eric Meier and Richard Milroy
University of Washington, Seattle, WA, USA

The Electrodeless Lorentz Force (ELF) thruster creates a high-density, magnetized plasmoid known as a Field Reversed Configuration (FRC) employing a Rotating Magnetic Field (RMF). The RMF driven azimuthal currents, coupled with the enhanced axial magnetic field gradient produced by the FRC inside the flux preserving conical thruster, produce a large axial JxB force that accelerates the plasmoid to high velocity. The ELF thruster has been demonstrated to successfully ionize and electromagnetically accelerate xenon, nitrogen, and oxygen propellants. This ability to utilize ambient gases enables a wide range of far-term applications that have not been explored. However, operation on lightweight gases at high thrust-to-power (low specific impulse and high efficiency) requires extremely low plasma formation and frozen flow losses. Neutral entrainment, an advanced and highly-efficient electromagnetic acceleration scheme is introduced. The initial investigation, modeling results, and theoretical framework for an advanced ambient propellant utilization technique, Neutral Entrainment, is introduced.

Nomenclature

e_k	=	Kinetic energy per atom [J]
$e_{k\text{-}ELF}$	=	Kinetic energy per atom due to the ELF thruster [J]
e_{ion}	=	Plasma formation energy per atom [J]
$e_{thermal}$	=	Plasma thermal energy per atom [J]
k	=	Boltzmann Constant
L_A	=	Interaction length scale [m]
m_0	=	Atomic mass [kg]
Z	=	Atomic ionization state [-]
N	=	Number of entrainment per atom
n_i	=	Ion density [m^{-3}]
T	=	Total temperature [K]
v_e	=	Average particle velocity [m/s]
ε_{ion}	=	Ionization potential [V]
η	=	Efficiency [-]
η_T	=	Total efficiency [-]
η_{PPU}	=	PPU efficiency [-]
η_{CE}	=	Charge exchange energy efficiency [-]
η_{NE}	=	Neutral entrainment energy efficiency [-]
$\lambda_{Ion\text{-}n}$	=	Ion-neutral collision length [m]
$\sigma_{charge\_exchange}$	=	Charge exchange cross section [m^{-2}]
$\sigma_{ionization}$	=	Ionization cross section [m^{-2}]
v_a	=	Relative collision velocity [m/s]

I. Introduction

The ability to utilize ambient orbital resources enables a wide range of far-term applications. Nearest term, an air-breathing, solar electric orbital transfer vehicle operating in a highly-eccentric Geostationary Transfer Orbit is possible that requires virtually no onboard propellant. While adding to spacecraft complexity, it allows for the effective utilization of many tons of ambient propellant. Additionally, ultra-high altitude, so-called Near Space propulsion is enabled for both high and low dynamic pressure applications (lighter-than air and hypersonic craft,

respectively). It is clear that being able to harness many tons available propellant without the requirement of launching would reduce cost, scale and size of spacecraft systems for missions that require large delta-V's and large amounts of propellants. In the orbital environments, it is believed that there are suitable nitrogen and oxygen resources from 80 to 200 kilometers altitude for use in plasma-based systems. The concept of utilizing atmospheric resources is not a new concept. Previous work has shown the orbital benefits of such effort [1], as well as Ion and Hall thruster modifications that would enable such utilization [2]. However, there are many challenges on both the thruster and systems level to utilizing in-situ atmospheric gases as propellants. While not addressed in this paper specifically, there are system level complications in collecting suitable amounts of propellants [3], as well as system integration concerns with requiring aerodynamic and drag considerations in spacecraft design.

From the thruster performance perspective, traditional electric propulsion technologies have several major concerns to utilizing oxygen and nitrogen molecules as propellants. First and perhaps most minor is that existing technologies require cathodes that are sensitive to oxygen interaction. Secondly in systems in which the plasma maintains extended contact with the thruster surfaces chemically reactive gases such as oxygen, nitrogen and hydrogen will tend to quickly erode and chemically sputter thruster surfaces even at low energies. Finally and most importantly, thruster efficiency is fundamentally a function of the molecular weight of the propellant and as will be shown in detail in later sections, it can be easily shown that for a given ionization energy cost (this includes both specific ionization costs, as well as thermal costs and wall losses) that efficiency decreases at the square root of the molecular mass which for traditional devices will dramatically reduce operational efficiency on light-weight gases even assuming successful operation. For missions in which propellant is being collected from the ambient atmosphere, the thrust provided by the thruster must overcome the drag induced by the propellant's collection. Similarly to combustion-based turbine propulsion systems. Therefore, optimal specific impulses for air breathing missions tend to be significantly less than for interplanetary or station-keeping missions. This effect is doubly challenging as the propellant mass is much smaller, while the mission need is for higher thrust.

Therefore, what is required is an electric propulsion system that can very efficiently ionize light weight gases, is completely electrodeless and has the ability to operate efficiently at low specific impulse and high thrust.

II. Description of Neutral Entrainment

A. Ionization Losses

Electric propulsion (EP) systems accelerate charged particles by the application of electrostatic and electrodynamic (magnetic) forces. In order to accelerate a propellant it must be charged and in typical electric propulsion systems it must undergo an ionizing collision event.

The primary loss mechanism for all fundamental non-thermal electric propulsion devices and technologies is plasma formation loss [4]. In a realistic EP system, it takes 100-500 eV/per atom to take one neutral propellant particle and eject one ionized particle not counting kinetic energy addition. All plasma-based electrostatic or electromagnetic propulsion systems require an ionized particle to be able to accelerate propellant at all. Fundamentally, the energy cost of an ionizing collision is quite small, on the order of 10-20 eV. This would roughly correspond with an accelerating voltage of 10-20V for 50% efficiency. However, this is not a realistic assessment of the total energy required for ionization. In real plasma, energy losses also include recombination, excitation (radiation), and polarization. These effects will tend to dominate the effect of the ionizing collision, specifically at low energies. Figure **1** shows a compilation of energy loss mechanisms for an ideal plasma in argon and oxygen which have minimum energies of ~14 and ~16 eV/ion. It's clear that for electron temperatures below 50 eV, the minimum total ionization potential is much greater than 14-16 V.

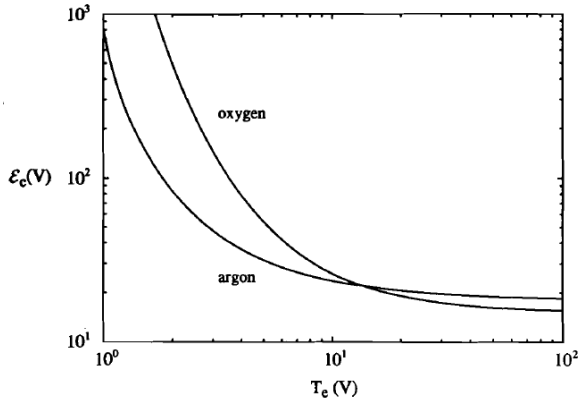

Figure 1. Ionization Energy costs including excitation for various electron temperatures [5]

Additionally, in a non-magnetized plasma the particles are free to collide with the wall thereby removing even more energy from the system. To directly compare with a hall thruster, Xenon has an ionization potential of 12 V/ion and operates with an electron temperature of 1-5 eV. The total collision cross section data was not available

for this document, however it is expected that at those electron temperatures the minimum ionization energy (ignoring wall losses) is > 100 eV/ion, based on the data in Figure 9. In fact, the measured ionization energy in a hall thruster typically optimizes to 150-200 eV/ion. Other electric propulsion devices can have even more dramatic losses [1].

For propulsion, the maximum thruster efficiency can be summed as the kinetic energy divided by the total energy spent (or power in a given unit of time). Equation 1 shows the efficiency as a function of propellant velocity, plasma temperature, and ionization energy.

$$\eta = \frac{E_K}{E_{Total}} = \frac{e_k}{e_k + e_{ion} + e_{thermal}} = \frac{\frac{1}{2} m_0 v_e^2}{\frac{1}{2} m_0 v_e^2 + e_{ion} + 2\gamma kT} \tag{1}$$

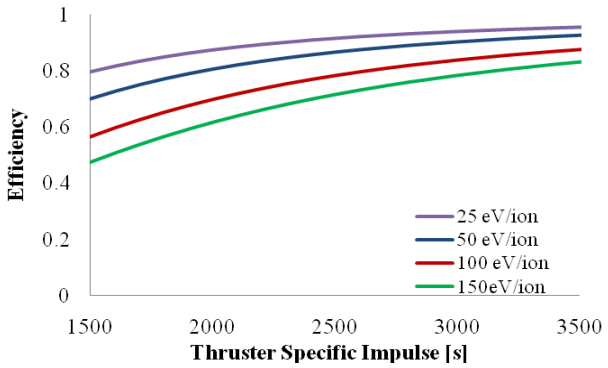

Figure 2. Theoretical efficiency as a function of specific impulse and ionization energy for Xenon

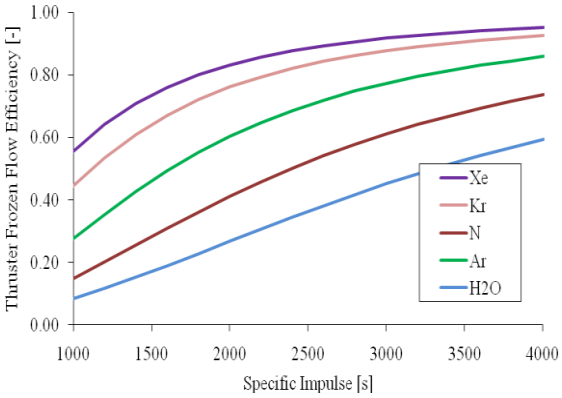

Figure 3. Theoretical efficiency as a function of molecular mass for 40 eV/ion

Using this equation a maximum theoretical efficiency can be calculated for various thruster configurations. Figure 2 and Figure 3 show the theoretical maximum propulsive efficiency for typical EP devices and propellants of interest. What will now be described is termed Neutral Entrainment and is believed to be a method of dramatically lowering the effective ionization costs for electric propulsion.

B. Neutral Entrainment

The fundamental concept in Neutral Entrainment (NE) is than a Field Reversed Configuration (FRC) will ingest large quantities of neutral gas through charge exchange collisions, not ionization. If you accelerate an FRC while providing upstream neutral gas, Isp can be specified and mass/thrust added with very high efficiency. In recent FRC experiments it was found that accelerating an FRC into and through a large neutral population was beneficial to the FRC [7]. It both gained mass and became more stable. Additionally, it is believed that only a fraction of these neutrals were ionized in the process, but most were swept up as the FRC passed.

Therefore, it is proposed to take the results of this discovery and apply it to a propulsion system. The Neutral Entrainment Study (NES) seeks to fully characterize, and finally optimize the neutral entrainment in a thruster environment.

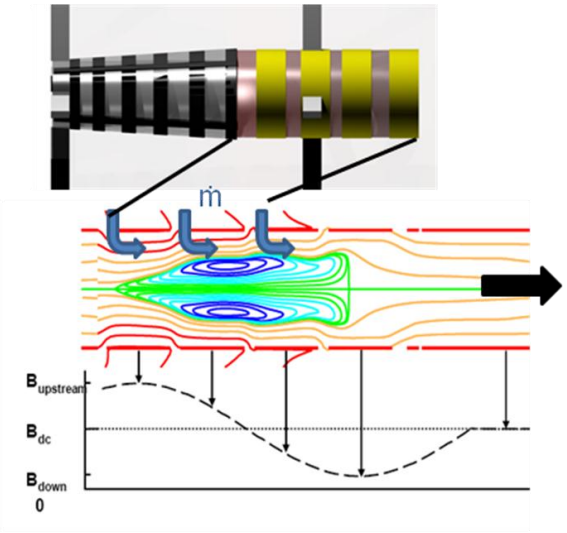

Figure 4. Neutral Entrainment ELF Thruster

Neutral entrainment is believed to occur as follows. A collisional, ionized propellant is accelerated in a gradient magnetic field, as in Equation 2. In this specific case it will be in the form of a closed field, isolated FRC that is translating in a constant bias magnetic field. A slow, cold neutral gas population is introduced in front of the

translating plasma. As the plasma ions collide with the neutral particles a positive ion will collide with an atom so as to capture a valence electron, resulting in a transfer of the electron from the atom to the ion. If this occurs between populations with the same mass, then the charge transfer occurs with *no* change in momentum. Additionally, kinetic energy is completely conserved. Equation 2 explains this concept, where P is a propellant atom. [4]

$$P^{+}(Fast)+P(Slow)\rightarrow P\ (Fast)+P^{+}(Slow) \tag{2}$$

Also, it has been shown that the collisional cross section for charge exchange is given as Equation 3 [7], where v_a is the relative velocity and ε_{ion} is the ionization potential.

$$\sigma_{CX}=\frac{1}{\varepsilon_{ion}}\left(\left(1.58*10^{-7}\right)-7.2*10^{-8}\ln v_a\right)^2 \tag{3}$$

After this collision the resulting fast moving neutral particle proceeds out of the thruster unhindered by magnetic fields and simply adds momentum. Meanwhile, the slow-moving charged particle is *still confined in an accelerating/gradient magnetic field* and is subsequently accelerated to high velocity and applying a thrust force to the spacecraft (via magnetic field coils). In total there are two fast moving, propellant particles but only one ionization loss, effectively reducing the total ionization loss per particle in half. Depending on the collision frequency, velocity, and density of the plasma and neutral populations this process will be repeated throughout an FRC and possibly several times. It is expected that there is a maximum of 8 neutral entrainments per particle possible with a typical NE geometry shown in Figure 4, reducing an ionization cost of 40eV/ion to 5 eV/ion, well below even the theoretical minima.

The key parameter in this analysis is the ratio of ionization to charge exchange collision cross section. As can be seen if Figure 5 the charge exchange collisions (in this case shown as Elastic) are always more likely than the ionization collisions. For the energies of interest charge exchange is 10 times as likely as ionization. Finally, even if there is a 10% population of ionized propellant particles, they are accelerated with the propellant and are not considered to be a loss.

There are several key parameters which must be met in order to optimize the entrainment of neutral particles in an accelerating field.

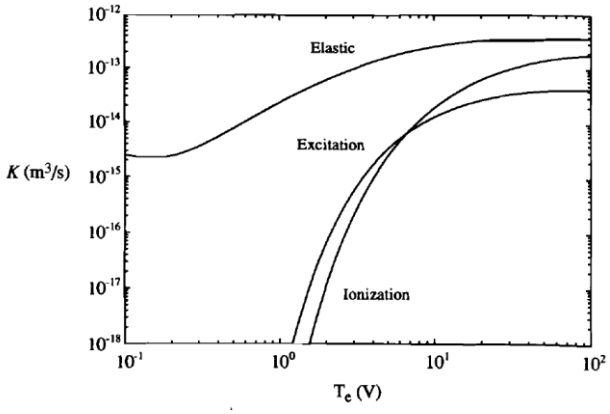

Figure 5. Collisional Reaction Rates

- High collision rate

In order to collide and entrain a neutral particle the mean free path must be significantly less than the interaction region. This requires that there be sufficient plasma density as well as neutral density. A generalized ion-neutral mean free path is described in Equation 4. This shows the dependencies which will dominate an ion-neutral collision rate that is typically empirically obtained. V is velocity, Z is charge state, T_i is ion temperature, μ is atomic mass ratio, and n_i is ion density.

$$\lambda_{Ion-n}=V/\nu_{i-n}\propto VZ^{-2}\mu^{1/2}n_i^{-1/2}n^{-1/2}T_i^{3/4}\quad [m] \tag{4}$$

Clearly for this application density, n_i and n must be large in order to interact on the scale of a thruster. Additionally, cold ions will be advantageous.

- Long acceleration region

  Equation 5 shows the minimum requirement for accelerator length. Additional collision would be beneficial in allowing multiple neutral entrainment interactions.

$$L_A > \lambda_{Ion-n} \tag{5}$$

- Cross Sections

Interaction temperature must be such that the charge-exchange collision cross section is larger than the ionization cross section. This is stated in Equation 6 is true for all plasmas of interest.

$$\sigma_{charge\_exchange} >> \sigma_{ionization} \tag{6}$$

- Body Forces and a Quasi-Neutral Plasma

The acceleration mechanism must be such that there is not interaction with the collision rates and plasma density. Additionally, the plasma must be quasineutral. These requirements lead directly to body forces and an electrodeless operation. If there are large internal plasma sheaths neutral entrainment may be compromised. Finally, the ability to choose a propellant based on collision cross sections (and use molecular propellants) would add significant propulsive and performance benefits.

And while most inductive and high density propulsion devices can be applicable to neutral entrainment *FRC plasmas fit these requirements perfectly and are the ideal test case for an experimental investigation of Neutral Entrainment.* Additionally, an FRC can be formed and translated into a region of only neutrals and accelerating field, creating an optimal geometry to study translation.

C. Summary of the ELF Thruster

The ELF creates a high-density, magnetized plasmoid known as a Field Reversed Configuration (FRC) using external RF antennas that produce a Rotating Magnetic Field (RMF) throughout the thruster, transverse to the thruster axis of symmetry in the r-θ plane. The synchronous motion of the electrons magnetized in this field produce a large azimuthal current, that when driven in a direction opposite to that flowing in the external solenoid, reduces and eventually reverses the magnetic field inside the plasma, thus forming a closed magnetic field configuration separate from the external thruster fields (the FRC). These large FRC plasma currents together with the greatly increased radial magnetic field created by the presence of the plasmoid result in a very substantial $J_\theta x B_r$ force that rapidly accelerates the FRC propellant out of the thruster (Fig. 1.). The axial force is thus overwhelmingly determined by the driven I_θ and resultant B_r rather than thermal expansion forces. However, as in any expanding magnetic field, the expansion of the FRC with the thruster cross section as it is ejected provides for the conversion of the FRC thermal energy into directed energy minimizing the frozen flow losses and maximizing efficiency. This thruster has been detailed in several other papers [8] and will only be described in brief as the FRC source for this application.

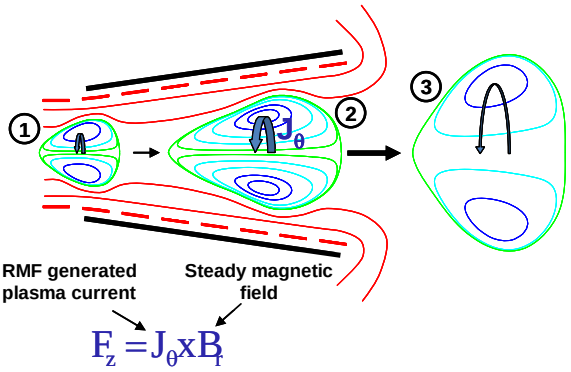

Figure 6. ELF Thruster Operation: (1) Rotating Magnetic Fields (RMF) form high-density, FRC plasmoid (2) FRC grows and accelerates driven by RMF generated currents & steady field (3) FRC expands as ejected, converting any remaining thermal energy into directed energy.

The technique of generating azimuthal electron currents in a plasma column by means of rotating magnetic fields was first investigated by Blevin & Thonemann in 1962 [7]. The principles of their technique can best be understood as follows. Consider that a transverse rotating magnetic field completely penetrates a cylindrical plasma column as in Figure 7. Provided that the angular frequency ω, of the rotating field lies between the ion and electron cyclotron frequencies (ω_{ci} and ω_{ce}) calculated with reference to the amplitude of the rotating field, B_ω, and provided that the electron collision frequency is much less than the electron cyclotron frequency, the electrons can be considered as 'tied' to the lines of force of the rotating field. With the assumption that the electron collisions are relatively infrequent ($\nu_e << \omega_{ce}$), they will circulate synchronously at the angular frequency ω, whereas the ions (at least over the time of interest) have no net azimuthal motion. The electrons thus form a steady azimuthal current (in fact, the Hall current). In most systems, Hall currents are inhibited by electric polarization fields. In the situation under discussion, however, charge separation does not occur because of the azimuthal symmetry.

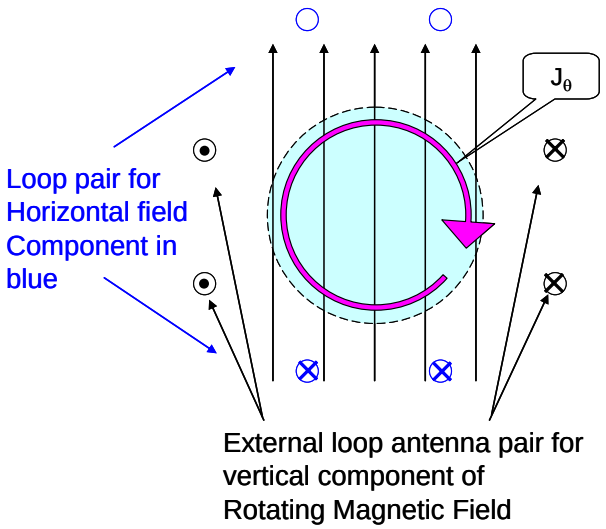

Figure 7. Schematic of the cross section of the plasma column and RMF lines of force. The coil set of axial conductors employed to generate the RMF are also shown. These two orthogonal sets, carrying sinusoidal currents phased 90° apart, produce an m=1 rotating magnetic field of constant amplitude.

It should be noted that the frequency condition for current drive:

$$\omega_{ci} < \omega < \omega_{ce} \tag{4}$$

The antenna geometry for generating the RMF are not unique to this application. In fact, the same antenna configuration and RF frequency requirements (Eq. 4) are found for the propagation of the helicon wave as well [10, 11]. The singular difference between the helicon discharge and the full electron entrainment found with FRC generation is the magnitude of B_ω. Both rely on the m=1 transverse mode penetrating the plasma and coupling to the electrons. This is accomplished with the rotating field in the case of a two phase antenna. The right hand circularly rotating component of the oscillating field produced by a single m=1 "saddle coil" antenna commonly employed for helicon discharges.

For the particular choice of field geometry and rotation frequency given in the above description, the appropriate form of Ohm's law is:

$$\mathbf{E} = \eta\mathbf{J} + -en(\mathbf{j} \times \mathbf{B}) \tag{5}$$

Steady-state solutions satisfying this equation can be obtained in two limits. In the limit of interest which leads to the formation of the FRC considers the **jxB** term in Ohm's law to be dominant. The solution in this limit was originally obtained by Blevin & Thonemann [9], which describes the penetration of the rotating field into the plasma column and is described by Eq. 6. Additionally, it can be shown that the change in external magnetic field when the Hall term is completely dominant and the electrons are all in synchronous rotation is given by Eq. 7.

$$j_\theta = -\frac{1}{\mu_0}\frac{\partial B_z}{\partial r} = -ne\omega r \tag{6}$$

$$\Delta B_z^M = B_z(r_p) - B_z(0) = \frac{\mu_0}{2\pi} e\omega N \qquad (7)$$

Thus it can be seen that a quite large azimuthal current as well as compressed field can be generated by a relatively low current rotating electric field. This is the key to efficient formation and electromagnetic acceleration of a plasmoid.

The ELF thruster that is being used as a source for the Neutral Entrainment study is shown in Figure 8. This particular embodiment is a 250 mm outer diameter and 420 mm length thruster. It has highly parallelized Litz wire antenna. Finally, in this thruster configuration each antenna phase is a simple L-C ring down oscillating circuit that use a 750 nF high Q RF capacitor and a high-power psuedospark switch from Pulsed Technologies LTD. All pulsed power hardware can be seen in Figure 9. For these tests the thruster was operated at a total power of 75 Joules with a Neon propellant as described below. Finally, all discharges and neutral gas puffs were evacuated into a large ballast chamber with a base pressure of 1E-7 Torr.

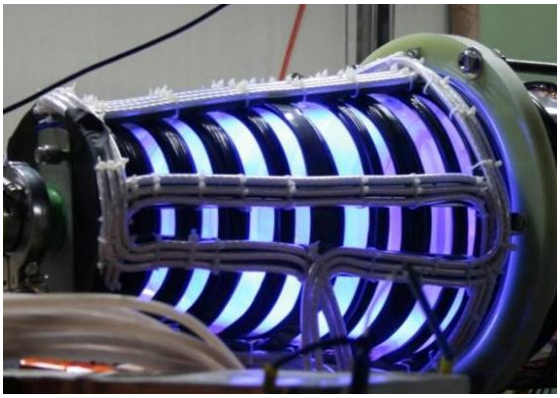

Figure 8. Neutral Entrainment Phase 1

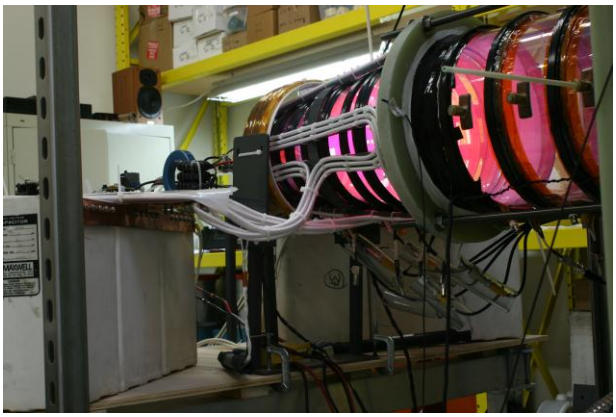

Figure 9. Neutral Entrainment Phase 1 operating with a 5E19 m^{-3} Neon discharge

III. Summary of Experimental Results

A. Neutral Entrainment Hardware Setup

Initial hardware testing was completed at MSNW of a neutral entrainment validation study. In Phase 1 of this study, which will be described here, the FRC is formed with a lightweight gas and accelerated out of a conical thruster. This FRC is then translated into a region with steady bias field coils and a neutral gas of specific distribution. By examining the motion and density and external magnetic field of the translating FRC with and without a neutral population, the effect of that background population can be determined.

The key hardware is shown in Figure 1 and consists of the 75 joule ELF thruster, drift neutral entrainment section, downstream ballast chamber and vacuum system as well as numerous probe ports. Perhaps the most important neutral entrainment hardware is the supersonic molecular beam injector (SMBI). The SMBI was designed to provide a high velocity low dispersion neutral puff to the downstream region. A high speed puff valve with 200 microsecond opening time injects gas into a 434:1 expansion Laval nozzle. This nozzle accelerates the high pressure gas from a 100 micron throat and accelerates and cools the gas to a theoretical Mach 18. A supersonic molecular beam differs from a traditional viscous supersonic nozzle in that at some location through the expansion nozzle the flow becomes kinetic and viscous affects are frozen out. Fundamentally, this can be seen as a radial cooling of the flow in which the radial velocity of a particle is reduced to the equivalent temperature of 10 to 20 Kelvin while maintaining an equivalent axial temperature. The supersonic molecular beam injector is shown in Figure 10 and Figure 11. Additionally, a coaxial pre-ionization electrode was designed that is coaxial with the

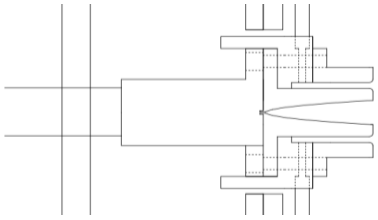

Figure 10. Supersonic Molecular Beam Injector Diagram. Shown is the inner supersonic nozzle, outer annular pre-ionization gas injector, and insulators.

supersonic molecular beam injector and provides gaseous injection for the FRC formation. The key advancements of this coaxial injector is that it utilizes a highly tangential injection scheme such that the axial velocity of the FRC propellant flow is dramatically reduced. This helps to both concentrate the gas for the FRC into the discharge region and separates the neutral beam from the primary propellant.

A fast ion gauge (FIG) was used to fully characterize the temporal and spatial neutral density distribution within the thruster and drift chamber regions for all relevant operating conditions. The neutral density distribution for the operating conditions described in this paper is shown in figure 3. What can be clearly seen in figure 3 is a radially compact, axially compact peaked neutral profile of the molecular beam as well as the uniform front of the incoming propellant from the thruster. These distributions are ideal for isolating and identifying the effects of neutral entrainment as well as validating the results from the code. It is believed that isolating the neutral flow from the chamber walls will help maximize propellant utilization and neutral entrainment effects.

Figure 11. Coaxial SMBI and pre-ionization electrode

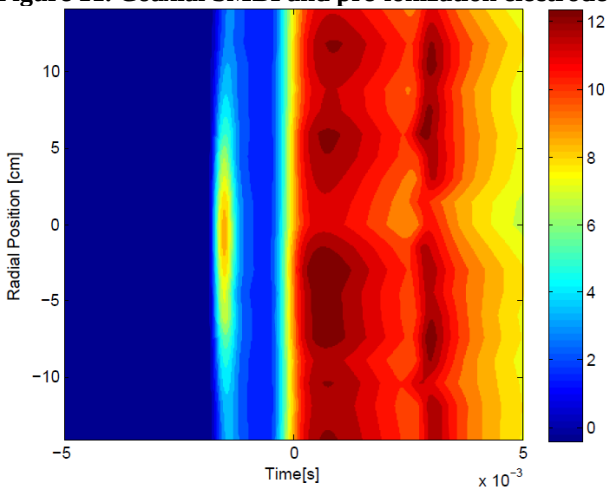

Figure 12. Neutral Density profile in mT for the discharge of interest showing initial neutral beam and follow-on FRC propellant flows.

B. Neutral Entrainment Experimental Results

A range of standard diagnostics is used to fully characterize a translating FRC. External magnetic field probes characterize the magnitude of diamagnetism and can directly yield the particle pressure of the FRC. Internal double Langmuir probes resolve transient plasma density at less than 1 microsecond resolution and have been arranged at several axial locations (as shown in the plot nomenclature). High speed current transformers yield instantaneous antenna and bias field magnet currents and thus the power absorbed by the plasma. And finally, external magnetic flux loops are used to characterize the total plasma trapped flux as well as flux leakage through the external flux conservers.

A standard FRC discharge is shown in Figure 13-Figure 15. Figure 13 shows the external excluded magnetic field for an FRC at various axial locations. What is shown is the increase in magnetic field that arises from the induced current in the FRC. Figure 14 shows the translating FRC as it drifts downstream in an axial bias field. Figure 15 shows the radial cross section and the temporal profile for a high density, translating FRC in the downstream, neutral entrainment region. It is clear that a coherent high-Beta plasma is present in the drift chamber, though it appears to be losing stability as it drifts through the downstream region.

From both the downstream magnetic field measurements as well as the Langmuir probe density measurements, an average velocity of the bulk plasma can be determined. Both agree quite excellently, and for the data shown here the FRC appears to be traveling at a an average 21 +/- 2 km/s throughout the drift chamber.

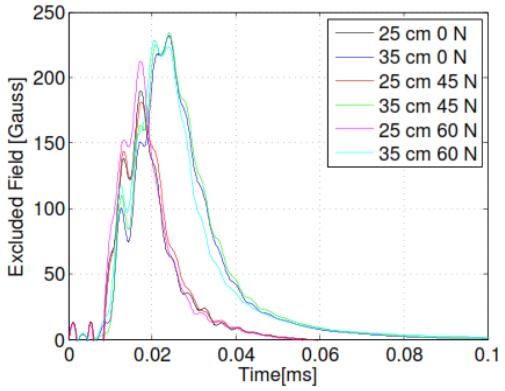

Figure 13. External excluded field for a 75 Joule Neon FRC.

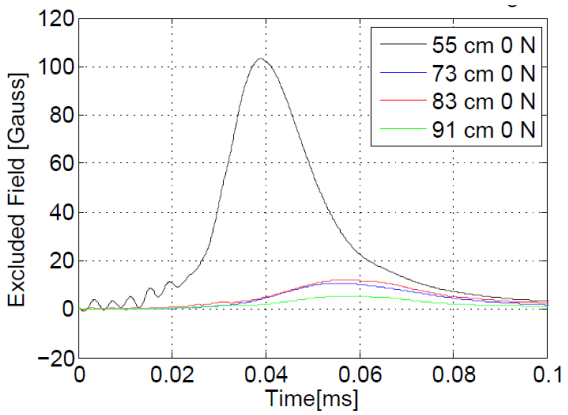

Figure 14. Downstream excluded field for a 75 Joule Neon FRC translating into a 50 Gauss field.

As described earlier, the neutrals for this study are injected through a high-speed supersonic molecular beam injector. The SMBI neutrals were added to the discharges above and the interaction was fully characterized. The location of the bulk neutral population was found to be moving at 812 m/s and was varied from near the thruster exit to well downstream in the ballast chamber. It must be noted here, that the primary difference between the modeling results shown later and the experimental conditions are in the final distribution of neutral flow. Unlike the model where discrete formation, drifting, interaction, and post-interaction drifting sections can be specified, in the experiments there will always be some smoothing of the boundaries of these regions. Figure 12 shows the actual neutral distribution throughout the ELF and neutral entrainment regions at the time of initial ELF formation. There is some small drift that occurs in the 40 microseconds it takes for the thruster to generate and accelerate the FRC into the drift chamber, but relative to the plasma traveling at 20 km/s, the neutrals are not moving.

Therefore, the neutrals were added to the discharge and complete profiles of external magnetic field and internal Langmuir probe measurements wear taken as above. In Figure 13, it can be clearly seen that the addition of the neutral beam does not interfere with the operation of the thruster within the thruster region. Shown is the external magnetic field results as before. In Figure 16, however, there are gross changes to the downstream characteristics of the translating plasmoid as shown by downstream magnetic field probes.

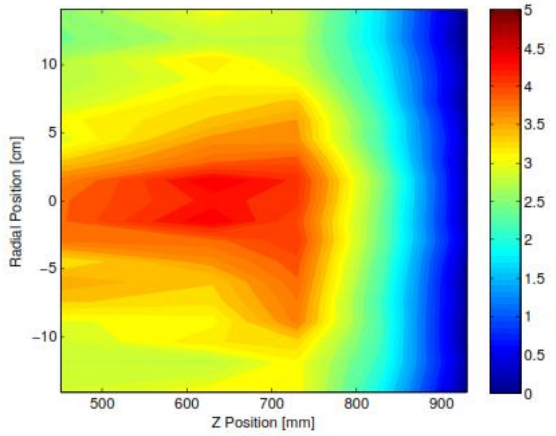

Figure 15. Spatial neutral density profile at the t=0, the time of RMF FRC initiation in mTorr.

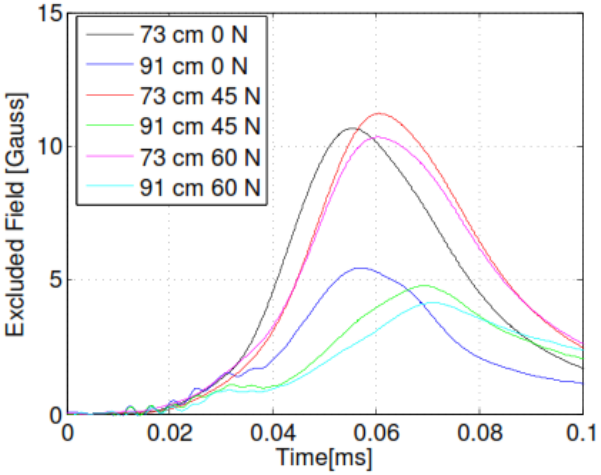

Figure 16. Comparison of excluded downstream magnetic field results for two locations with and without a neutral beam (NB).

Figure 17, Figure 18, and show comparisons of downstream plasma density. It is clear from this data that the FRC is interacting with the background gas in the required way. Plasma density increases somewhat, while the

bulk velocity clearly decreases from 21 to 15 km/s (taken at 4 cm) for increasing neutral density. Also, it can be seen that the bulk velocity decreases throughout the drift region. And finally, and perhaps most importantly, it can be seen that the plasma diamagnetism does not decrease due to the background effect of the neutrals, infact there is some increase in measured excluded field. This is highly indicative that not only did the plasma currents remain during the entrainment process, but in fact the FRC expanded and perhaps gained some plasma mass during the process. At this point it is clear that the experimental results line up qualitatively quite well with the modeling results and shows that in fact the plasmoid appears to have successfully entrained a large quantity of neutrals with only minor ionization and radiation losses.

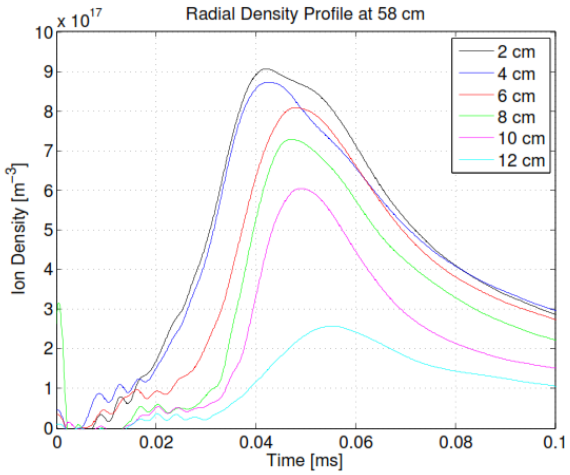

Figure 17. Radial FRC profile

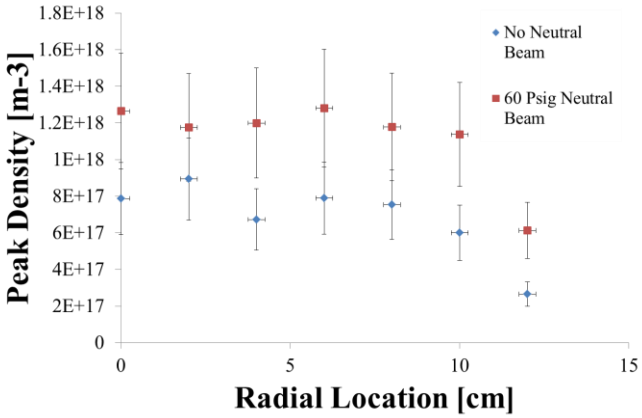

Figure 18. Comparison of temporally resolved density profile at two neutral beam pressures at 58 cm downstream

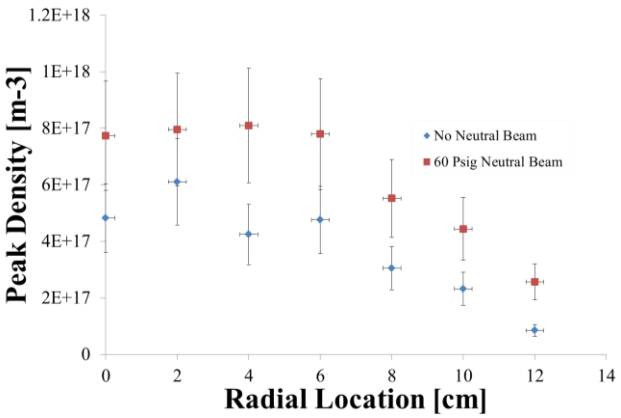

Figure 19. Comparison of temporally resolved density profile at two neutral beam pressures at 78 cm downstream.

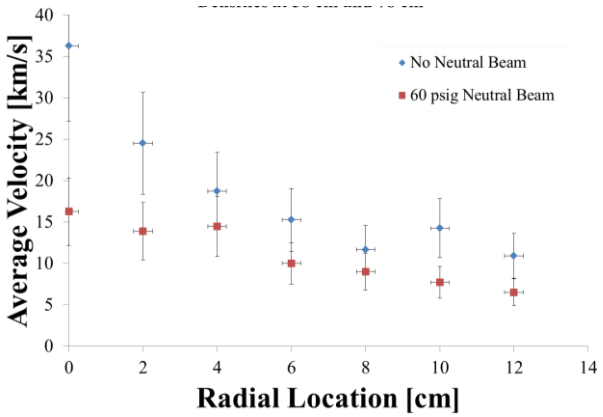

Figure 20. Comparison of temporally resolved density profile at two locations

I.V. Summary of Modeling Results

The Plasma Science and Innovation Center (PSI) at the University of Washington has developed a two-fuid model of interaction plasma and neutral fluids[12]. This model is based on the SEL-HiFi code [13], a 3D MHD code with advanced features that are ideal for modeling this complex interaction. SEL-HiFi uses a flux-source form for inputs, is completely implicit with an adaptive grid with high-order spectral elements. To this code Dr. Meier as added the capability to investigate a neutral fluid with resonant charge exchange, electron-impact ionization, and radiative recombination reactions. Braginskii closures are used for the plasma, and Chapman-Enskog hard sphere closures are used for the neutral gas. And while experimental validation is on-going with the latest experimental results, presented here is a summary of results obtained from early simulations runs and presented at the 2011 Innovative Confinement Concepts meeting.

Figure 21 and Figure 22show results from a propagating FRC interacting with a background neutral gas. In these cases, the total plasma mass of the FRC and neutral mass of the interaction region are equal. Additionally, the neutral mass is centered on axis as in the experiment and extends for 50 cm downstream. In these simulations a 30 microgram FRC is colliding with a 30 microgram Neon region after being initialized to 26 km/s axial velocity. Figure 21 shows the neutral density and momentum during the FRC interaction. It is clear that the FRC compresses and accelerates the neutral propulsion. Additionally, there is evidence of some ionization of the neutral gas. Figure 22 shows the plasma pressure increase as the FRC interactions with the neutral pressure. Finally, as you would expect, there is an increase in diamagnetism and a slowing of the FRC as it passes through the gas.

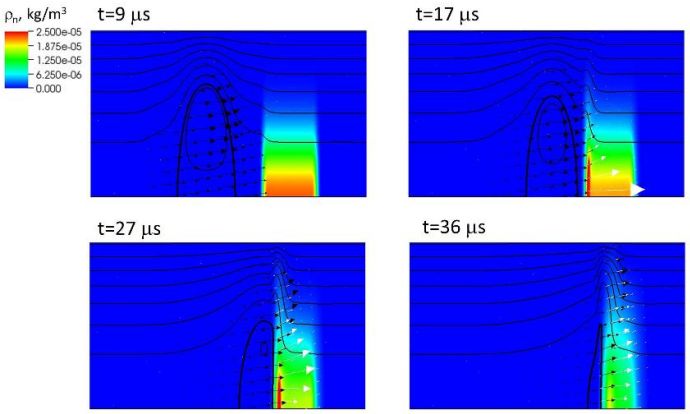

Figure 21. Neutral density psuedocolor plots for baseline ELF simulation with a Gaussian radial neutral gas profile. Black and white arrows indicate the direction and magnitude of plasma and neutral momentum, respectively. Clear neutral entrainment is seen.

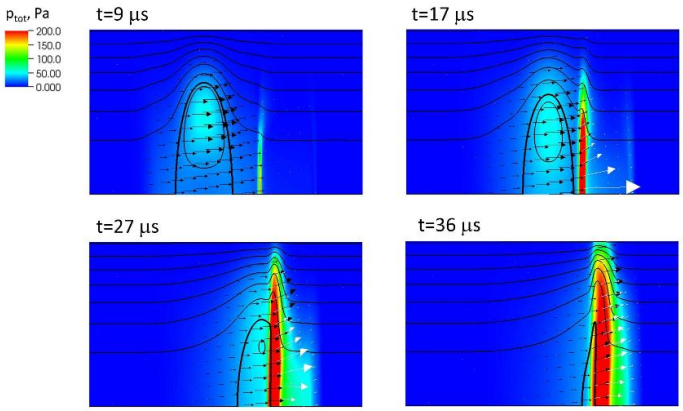

Figure 22. Pressure psuedocolor plots for baseline ELF simulation. Clear neutral entrainment, pulse sharpening, and increase in external magnetic field pressure are seen.

Figure 23 and Figure 24 show temporal profile of the total momentum and energy components of the FRC as well as the neutral population. Again, this is for a case in which the neutral mass was equal to the plasma mass. Quite obvious from these results is that both charge exchange and ionization play a critical role in these processes and that momentum can successfully be transferred to the neutral gas as desired. For an equal plasma to neutral mass, approximately 50% of the momentum of the plasma is transferred to the plasma, with a majority of that momentum transfer coming from charge exchange. In these cases, it appears that there is significant ionization of the background plasma although that energy appears to mostly come from the initial thermal energy of the plasma rather than the kinetic energy, exactly as desired. And while not a loss mechanism in neutral entrainment as the new plasma will be accelerated with the initial FRC plasma, this is less neutrals entrained overall, lessening the efficiency and T/P gain. Additionally, it was found that the amount of ionization was directly the result of the temperature of the final, expanded translating FRC. At very high temperatures (20 eV or above) it was found that 90% of neutrals may be ionized in entrainment. For 5 eV total temperatures (similar to experiments) and high downstream neutral density it was found that as low as 20% of neutrals are ionized while 80% of the plasma momentum is transferred to the neutrals.

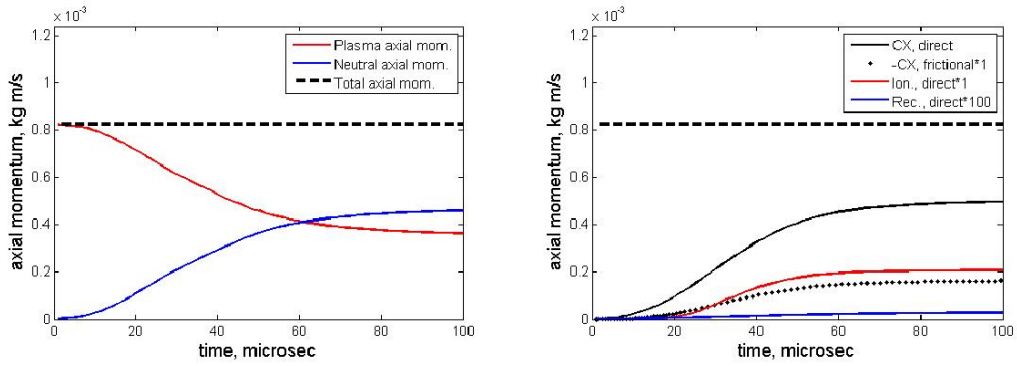

Figure 23. Temporal profiles of momentum-related quantities for ELF baseline simulation

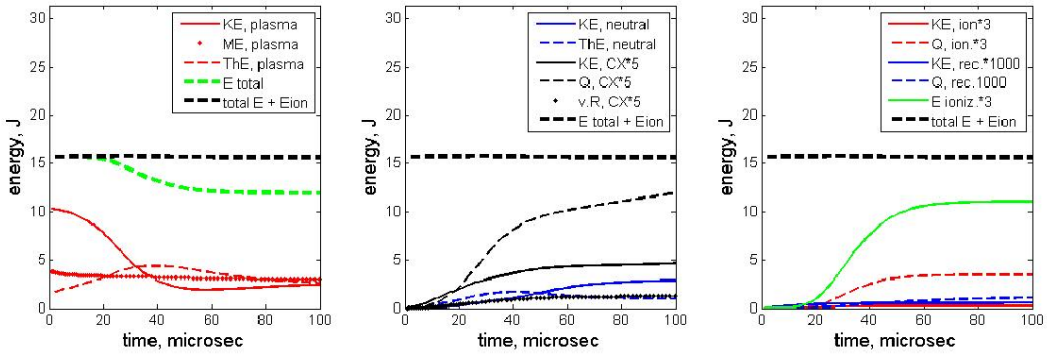

Figure 24. Temporal profiles of energy-related quantities for ELF baseline simulation

V. Neutral Entrainment Discussion

The neutral entrainment phase 1 tests have demonstrated that the ELF thruster can be successfully operated in Neon. FRCs were created with 30 to 75 Joules and translated greater than one meter. The ELF thruster demonstrated up to 4000 seconds specific impulse and was was fired for 3000 discharges with zero erosion or wall effects. Additionally, well-formed, fully excluded FRCs were reliably created with lifetimes on the order of 100 microseconds and fully reverse magnetic profiles. Figure 13 through Figure 16 showed the plasma characteristics of a neon FRC.

Neutral entrainment was added to the ELF thruster by use of a supersonic molecular beam injector that allowed for highly localized addition of neon propellants to the downstream region of thruster interaction. Figures 17 through 24 showed the resultant FRC and estimates of the interaction results. It was clear that the neutral density had significant effects on the plasma and appeared to have demonstrated all of the expected qualitative effects as have been seen in the early modeling results. The FRC interacted with the background gas and was decelerated by that gas. It also appears that some small amount of ionization occurred and that this ionization was initially at the leading edge of the FRC and then propagated until the radial expense of the FRC, also as expected. Additionally, it appears that mass was added to the plasma in the form of charge exchanged neutrals and momentum (approximately 50% of the initial FRC momentum) was added to this neutral population. While it is not clear at this time what the actual and total conversion efficiency was it is clear that expected loss mechanisms, such as wall collisions and radiation losses were not observed as shown by the Langmuir probe results and additionally high-speed downstream photography of the neutral emission spectra.

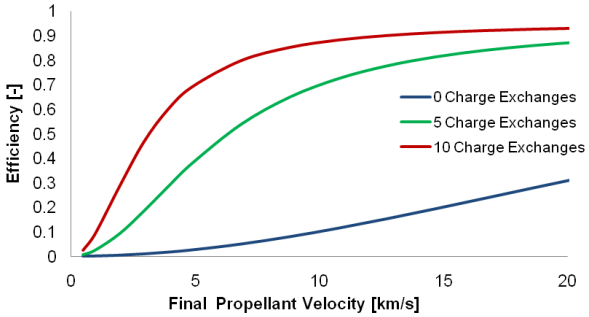

Figure 25. Theoretical thruster efficiency for a 40 eV/ion Nitrogen thruster as a function of increasing average charge exchange collisions and final propellant velocity in a Neutral Entrainment system.

Equation 1 gave a simple and clear thruster efficiency derivation for a given plasma formation energy (regardless of the complex sources of the energy loss). This can be extended to Equation 8 which includes N, for the number of neutral entrainment collisions a particle undergoes. Also included are the charge-exchange and neutral-entrainment conversion efficiencies. It must be made clear that implicit in this discussion is that there is subsequent kinetic energy added to the propellant (with an efficiency given by η_{PPU}) in order to accelerate the gas to its final velocity. Figure 25 shows a representative chart of theoretical thruster efficiency based soley off of the plasma formation energy loss, frozen flow losses, and neutral entrainment magnitude. While this doesn't include all of the various minor loss mechanisms (PPU, magnets, etc) that one would expect in a total thruster system this shows the dramatic capability improvement for high thrust-to-power operation of a neutral entrainment system on lightweight propellants.

$$\eta_T = \eta_{PPU} \frac{e_{k-ELF} + \eta_{CE}\eta_{NE} N e_k}{e_{ion} + e_{thermal} + e_{k-ELF} + \eta_{CE}\eta_{NE} N e_k} \tag{8}$$

Phase 2 will seek to add acceleration stages to the neutral entrainment experiment in order to demonstrate the increase the resultant thruster efficiency. In summary, the neutral entrainment Phase 1 experiment is a success and the authors believe that this technology has the possibility to enable efficient and high-thrust operation of electric propulsion systems on lightweight and molecular gases. The authors would like to thank the Air Force Office of Scientific Research for support of the Neutral Entrainment program.

References

[1] Nishiyama, K., “Air Breathing Ion Engine”, Twenty-Fourth International Symposium on Space Technology and Science (2004).

[2] Wahl, E.L., “Air-breathing electrostatic ion thruster “,US Patent App. 20,080/028,743 (2006)

[3] McGuire, T., “Aero-Assisted Orbital Transfer Vehicles Utilizing Atmosphere Ingestion”, MIT Thesis (1999).

[4] Jahn, R. Physics of electric propulsion, McGraw-Hill, 1968.

[5] Lieberman, M. and A. Lichtenberg. Principles of plasma discharges and materials processing, Wiley (2005).

[6] Matsuzawa, Y., et. al, “Effects of background neutral particles on a field-reversed configuration plasma in the translation process”. Physic of Plasmas 15 (2008).

[7] Rabb, D. and W. Francis. "Charge exchange between gaseous ions and atoms." The Journal of Chemical Physics 37: 2631, 1962.

[8] J. Slough, D. Kirtley, and T. Weber. “The ELF Thruster”. IEPC 2009-265 (2009).

[9] H.A. Blevin and P.C. Thonemann, “Plasma Confinement using an Alternating Magnetic Field”, Nucl. Fus. Suppl. Part I, 55 (1962).

[10] Francis F. Chen, “Physics of helicon discharges”, Phys. Plasmas 3, 1783 (1996).

[11] Yasuyoshi Yasaka and Yoshiaki Hara, “Role of Helicon Waves on High-Density Plasma Production”, Jpn. J. Appl. Phys., 33 5950 (1994).

[12] Meier, E.T., et al. "Development and validation of a two-fluid plasma-neutral model", Innovative Confinement Concepts (2011).

[13] A.H. Glasser, X.Z. Tang, Comput. Phys. Commun. 164 (2004) 237